The role of protolith composition in the formation of tin-enriched granitic melts: A modeling study using the example of the southwest China tin province

Yongchao Liu [a,b], Christian Schmidt [b], Jiankang Li [a,*], Denghong Wang [a], Qinggao Yan [c], Jessica A. Stammeier [b], Melanie J. Sieber [b,d]

[a] MNR Key Laboratory of Metallogeny and Mineral Assessment, Institute of Mineral Resources, Chinese Academy of Geological Sciences, Beijing 100037, China
[b] GFZ German Research Centre for Geosciences, Telegrafenberg, 14473 Potsdam, Germany
[c] Kunming University of Science and Technology, Kunming 650093, China
[d] Mineralogy, Institute of Geosciences, University of Potsdam, Karl-Liebknecht-Straße 24–25, 14476 Potsdam, Germany

ARTICLE INFO

ABSTRACT

Important features of Sn mineralization are the heterogeneous geographic distribution and frequent regional separation from W mineralization in spite some similarities of Sn and W behavior during magmatic processes. Major Sn and W mineralization is often spatially associated with peraluminous granites, which are derived from partial melting of metasediments. Several concepts have been suggested to explain those features, such as a weathering-related Sn-enriched source, Sn redistribution between melts and restite during protolith melting, and extensive fractional crystallization. We demonstrate the importance of protolith composition for the formation of Sn (and W) granites by using a comprehensive bulk-rock composition dataset from Precambrian metasediments of the South China Sn-W province and employing a thermodynamic modeling approach. We used four compositional proxies for phase equilibria calculations, which are the metasediments of the Mengdong, Sibao, Pingbian, and Shuangqiaoshan Groups. It is well documented that those Precambrian metasediments are important protoliths of Sn granites in South China. We present quantitative evaluation of the control of protolith composition in the generation of Sn-enriched granitic melts using South China as example, but our conclusions may also be applicable to worldwide Sn–enriched granites. Our results indicate that the protolith major-element geochemistry controls the anatectic reactions and melt productivity at specific melting conditions, and consequently the partitioning behavior of Sn. Further, pre-enrichment of Sn is crucial to the fertility of granitic melt and may be a prerequisite, particularly for the formation of giant Sn deposits. We propose that the heterogeneous distribution of favorable source rocks is one of the important factors that control the spatial distribution of major Sn (and W) districts in South China and other regions worldwide.

1. Introduction

More than 99 % of global cumulative historic tin (Sn) production is from ore deposits directly or indirectly related to granitic rocks (Lehmann, 2021). Tin mineralization is usually in spatial association with peraluminous ilmenite-series granites (Ishihara, 1981; Lehmann, 1990). Multiple processes are thought to play a role in the formation of Sn deposits (Carr et al., 2021; Romer et al., 2022). These include: (1) residual enrichment of Sn due to intense chemical weathering on a stable continent, transport of these sediments to a passive continental margin,

stacking of the shelf sediments and collision in an active margin (Romer and Kroner, 2015; Romer et al., 2022), (2) partial melting of subducted metasediments (Romer and Kroner, 2015; 2016) with partitioning of Sn into the granitic melt (Taylor and Wall, 1992; Wolf et al., 2018), (3) Sn enrichment due to magmatic fractionation (Ishihara, 1977; Lehmann, 1990) and assimilation (Carr et al., 2021), (4) exsolution of aqueous chloridic fluid from the granitic melt and hydrothermal alteration of Sn-bearing granite and wall rocks (Schmidt, 2018; Schmidt et al., 2020; Carr et al., 2021), and (5) deposition in pegmatites by crystallization from the melt, mineralization due to metasomatic reactions (skarn,

greisen, and sulfide replacement type deposits), and in vein deposits by several possible processes (Lehmann, 1990; Heinrich, 1990; Korges et al., 2018; Schmidt, 2018).

Tin mineralization is associated with the same type of granite as W mineralization. However, locally and regionally, Sn mineralization is commonly separated from W mineralization. This means that Sn and W mineralization often occurs in the same deposit, although usually either

Sn or W predominates over the other (Romer and Kroner, 2016; 2022; Zhang et al., 2017a; Schmidt et al., 2020). On the scale of intrusions and deposits, the predominance of one metal over the other has been attributed to the fractional crystallization and melt-hydrothermal transition processes (e.g., Heinrich, 1990; Lehmann, 1990; Korges et al., 2018; Schmidt et al., 2020). On the regional scale, different explanations exist for the heterogeneous distribution of major Sn and W
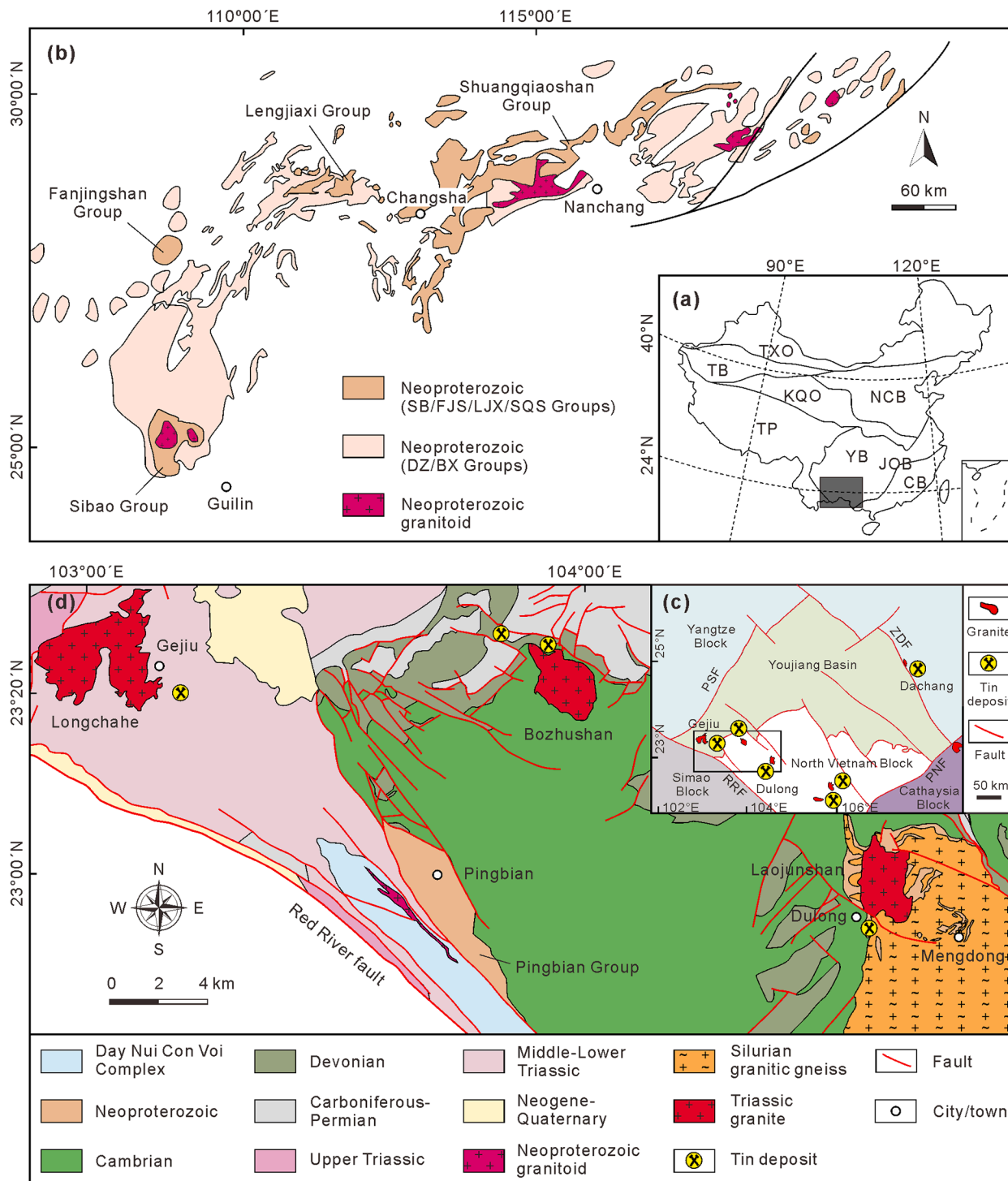
Fig. 1. Simplified geological maps showing (a) the major tectonic units in China, (b) the distribution of Precambrian basement rocks in the Jiangnan Orogenic Belt (JOB), (c) the distribution of Precambrian basement rocks, Cretaceous granites and related Sn deposits in the Youjiang basin (grey area in (a)), and in the southeast Yunnan region (d) (modified from Wang et al., 2012; Mao et al., 2013; Liu et al., 2020; 2021; Li et al., 2021). TKO Tianshan-Xingmeng Orogen, TB Tarim Block, KQO Kunlun-Qinling Orogen, NCB North China Block, TP Tibetan Plateau, YB Yangtze Block, CB Cathaysia Block. Sedimentary groups: SB Sibao, FJS Fanjingshan, LJX Lengjiaxi, SQS Shuangqiaoshan, DZ Danzhou, BX Banxi. RRF Red River fault, PSF Panxian-Shizong fault, ZDF Ziyun-Du'an fault, PNF Pingxiang-Nanning fault.

mineralization. Melting temperature of source rocks has been proposed to be responsible for the regional separation of Sn and W mineralization (Simons et al., 2017; Wolf et al., 2018; Yuan et al., 2019; Zhao et al., 2022). However, the differences in composition and/or Sn contents of source rocks were not considered by these authors. Early models show that the protolith composition, namely chemically intensely weathered rocks, may contribute significantly to the geographical distribution of Sn and W mineralization (Romer and Kroner, 2015; 2016; Romer and Pichavant, 2021). Song et al. (2022) argued that the difference in magma source material, resulting from previous episodes of high-grade metamorphism or low-temperature melting, may play a critical role in the separation of Sn and W mineralization across the South China Sn-W province. Furthermore, a recent model suggests that pre-enrichment of Sn by mobilization from sediments during prograde metamorphism may be an important step towards the formation of Sn-enriched melts and, thus, the spatial distribution of Sn districts (Romer et al., 2022). Here, we demonstrate quantitatively to which extent the source rock (meta-sediment) composition and pre-enrichment of Sn are relevant in the formation of granite-related Sn (and W) mineralization. For this study, we focus on South China, for which regional separation of Sn and W mineralization is well documented and the relation between exposed metasediments and granites has been established in previous studies (e. g., Yu et al., 2023). This provides an ideal opportunity to investigate the role of protolith composition and Sn (and W) pre-enrichment in the formation of one of the most important Sn-W provinces in the world, with the largest currently known Sn and W resources (Yang et al., 2018; Mao et al., 2019; Han et al., 2021; USGS, 2023). To this end, we combine published and new geochemical data of metasediments from South China with thermodynamic modeling, but our findings may be applicable to worldwide deposits.

2. Geologic setting

In the South China Sn-W province, most of the Sn mineralization occurs in the western part, including the giant Gejiu (reserve and grade: 3.0 Mt Sn at 0.8 wt%), Dachang (0.88 Mt Sn at 1.79 wt%), and Dulong (0.33 Mt Sn at 0.34–0.57 wt%) deposits in the Youjiang basin. The W mineralization is located mainly in the eastern part, including the giant Zhuxi (3.44 Mt WO$_3$ at 0.54 wt%), Dahutang (1.07 Mt WO$_3$ at 0.15 wt %), Xianglushan (0.22 Mt WO$_3$ at 0.64 wt%), and Dongping (0.20 Mt WO$_3$ at 0.45 wt%) deposits in the Jiangnan Orogen. The distribution of major Sn-W deposits in South China has been shown in previous studies (e.g., Fig. 1 in Mao et al., 2013; Fig. 1 in Yu et al., 2023).

The Youjiang basin lies in the southwestern part of South China, bounded by the Red River fault in the southwest, the Panxian-Shizong fault in the northwest, the Ziyun-Du'an fault in the northeast, the Pingxiang-Nanning fault in the southeast, and extends to northeastern Vietnam to the southwest (Fig. 1). The exposed stratigraphic units in the area are mainly composed of 1) Cambrian to Ordovician terrigenous-carbonate and clastic sediments, 2) Devonian to Permian limestone, siliceous limestone, and clastic rocks, and 3) Triassic turbiditic sediments (Mao et al., 2019). Granitic plutons are mainly emplaced along the margin of the Youjiang basin during the Late Cretaceous (~90–80 Ma) and are commonly associated with Sn mineralization (Cheng et al., 2016; Guo et al., 2022). The southeastern Yunnan Sn districts are located in the southwestern margin of the Youjiang basin, including the Gejiu, Bainiuchang, and Dulong Sn deposits, which are associated with the Longchahe, Bozhushan, and Laojunshan granites, respectively (Cheng et al., 2016). The Dachang Sn district lies in the northeastern margin of the Youjiang basin, which is related to the Longxianggai granite (Guo et al., 2022). These S–type, Sn-enriched granites are believed to result from partial melting of Precambrian metasediments (Cheng and Mao, 2010; Chen et al., 2015; Xu et al., 2015; Zhao et al., 2018; Guo et al., 2022).

We focus on the Precambrian basement rocks in southwest China, because they provide a unique opportunity to study the role of source

rock composition in the formation of Sn-granites in the major Sn province of South China. These rocks include the Mengdong and Pingbian Groups in the Youjiang basin and the Sibao Group in the Jiangnan Orogenic Belt (Fig. 1). For comparison, we compiled published chemical data of the Shuangqiaoshan Group in the southeast China W province, likewise in the Jiangnan Orogenic Belt. The Neoproterozoic Sibao Group (low greenschist facies) is the main exposed Precambrian metamorphic rock in the southwestern part of the Jiangnan Orogen. The Sibao Group is divided into the Jiuxiao, Wentong, and Yuxi Formations from the base upward: the Jiuxiao Formation is composed mainly of sandstone, *meta*-siltstone, quartz-sericite phyllite, and mudstone with mafic interlayers; the Wentong Formation mainly consists of sandstone and siltstone; the Yuxi Formation is composed mainly of *meta*-pelitic siltstone, siltstone, mudstone, and sandstone (Wang et al., 2012; Yan et al., 2019). It should be noted that the metasediments of the Sibao Group are also the main exposed lithology in the Jiuwandashan-Yuanbaoshan Sn domain, where more than 30 Sn deposits have been explored, including the large Jiumao and Yidong-Wudi deposits (Mao et al., 2019). The main exposed Precambrian basement rocks in the Youjiang region are the Neoproterozoic Mengdong and Pingbian Groups (Figs. 1 and 2). The Mengdong Group occurs as large irregular bodies or relicts in map view associated with high-temperature metamorphism-deformation (Fig. 2; Tan and Liu, 2017a; Liu et al., 2021). The Mengdong Group is reported to be metamorphosed up to lower amphibolite facies and consists of the lower Nanyangtian unit and the upper Saxi unit (Liu et al., 2000; Tan and Liu, 2017b). The Nanyangtian unit is dominated by mica schist interbedded with gneiss and amphibolite, and the Saxi unit is mainly composed of leptynite and quartzite. It has been demonstrated that the Mengdong Group has an affinity with the Neoproterozoic basement rocks in the Yangtze Block and shows characteristics of similar provenance to the basement rocks, e.g., in the Sibao-Fanjingshan area, southwest China (Zhou et al., 2018). The Pingbian Group is exposed in
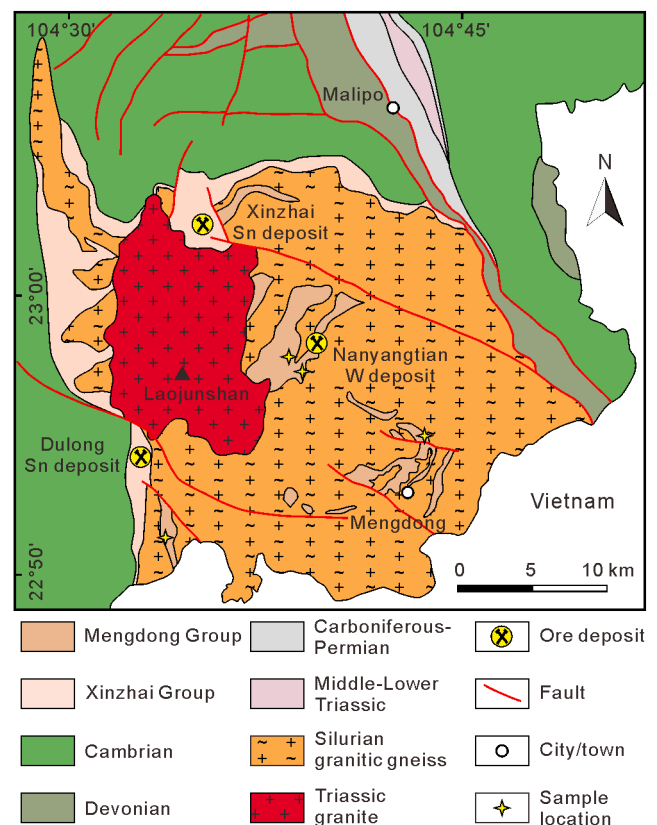

Fig. 2. Simplified geological map of the Laojunshan area in southwest China (modified from Que, 2016; Liu et al., 2021).

the area between Gejiu, Bozhushan, and Laojunshan granites, near the southeastern section of the Ailaoshan-Red River strike slip shear zone. The Pingbian Group has only undergone low-grade metamorphism and has a high proportion of siliceous component, mainly consisting of *meta*-sandstone, slate, and phyllite. The rocks mainly contain quartz, feldspar, and sericite. The geochemical and petrologic characteristics of Pingbian Group are similar to those of the low-grade Neoproterozoic basement rocks in the Yangtze Block (Zhu et al., 2019).

3. Methods

We compiled published bulk-rock geochemical data for the metasediments of Mengdong, Sibao, and Pingbian Groups in southwest China Sn province, as well as for the Shuangqiaoshan Group in southeastern W province for comparison. In addition, we sampled and investigated four fresh Mengdong mica schist samples from outcrops in the Laojunshan-Song Chay area (sampling locations are shown in Fig. 2), because giant Sn deposits like the Dulong deposit are located in this area. The samples are mainly composed of quartz, biotite, muscovite, plagioclase (Fig. 3) plus chlorite, garnet, aluminosilicate, and accessory minerals (Fe-Ti oxides, apatite, zircon, tourmaline). The samples were crushed to 230-mesh powders for whole-rock elemental analyses. The bulk major and trace element compositions were determined by XRF and ICP-MS at the ElMiE-Lab, at the German Research Centre for Geosciences (GFZ) Potsdam. Major elements were measured on fused beads with an AXIOS advanced spectrometer (Malvern Panalytical, UK). Loss of ignition (LOI) was determined by weight difference after fusion. For ICP-MS analysis, samples were digested using the 4-acid method (hot aqua regia/HF/HClO$_4$) in Savillex® PFA beakers (Savillex Corp., Eden Prairie, USA) using ultrapure reagents. The diluted digests were then measured using high resolution ICP-MS (ELEMENT 2XR, Thermo Scientific, Waltham, USA). The quantification level was 0.02 wt% for major elements and 1 ppt for Sn.

The average compositions (based on available data as compiled in Appendix Table A1) for the Mengdong mica schist, the metasediments of Sibao Group, and Pingbian Group from southwest China Sn province, and Shuangqiaoshan Group from southeast China W province were used for modeling. Note that some data within each group that are obviously inconsistent were eliminated from the dataset. It should be pointed out that variations in bulk composition may affect the absolute position of phase assemblages in *P-T* space (Johnson and Brown, 2004). Thus, it is likely that the overall topology of the phase diagrams is representative even if the average compositions of the studied metasediments are not fully representative. Thermodynamic modeling was performed using the GeoPS software, an interactive visual computing tool for thermodynamic modeling of phase equilibria (version 3.4, Xiang and Connolly, 2021), which minimizes the Gibbs free energy of the system, and the internally consistent mineral thermodynamic database (hp62ver.dat, Holland and Powell, 2011). The phase diagrams were constructed for the system of Na$_2$O-CaO-K$_2$O-FeO-MgO-Al$_2$O$_3$-SiO$_2$-H$_2$O-TiO$_2$

(NCKFMASHT). The amount of H$_2$O involved in the calculation was adjusted to be consistent with hydrated subsolidus mineral assemblages undergoing fluid-absent melting (e.g., Garcia-Arias and Stevens, 2017; Wolf et al., 2018), because partial melting of the crust takes place predominantly under fluid-absent conditions (Clements and Vielzeuf, 1987). Manganese was ignored in the modeling because of its low content (averages less than 0.1 wt%) in the natural samples. We follow the rationale established by previous studies (e.g., Wolf et al., 2018) and treat all iron as ferrous iron for reducing conditions. This is in line with the observations that Sn-granites are formed at relatively reducing conditions (Lehmann, 1990). Based on the geochemical characteristic of studied samples, the considered phases and activity–composition (*a–x*) models include chlorite, garnet, mica, cordierite, biotite, chloritoid, staurolite, orthopyroxene, melt (White et al., 2014), ilmenite (White et al., 2000), spinel (White et al., 2002), and feldspar (Fuhrman and Lindsley, 1988). Aluminosilicate, rutile, quartz, and H$_2$O are treated as pure phases. Uncertainties on the positions of phased assemblage boundaries are thought to be within ± 50 °C and ± 1 kbar (Palin et al., 2016). The contents of minerals and melt and corresponding melt compositions at the conditions of 800 °C, 4 kbar and 800 °C, 7 kbar were calculated in order to quantify the distribution of Sn during partial melting of metasediments. The choice of the temperature (*T*) is based on the reported data of zircon-saturation thermometry for Sn-granites that show high melting temperatures, i.e., ~800 °C (Zhao et al., 2022) and for the less evolved Laojunshan granites in the southwest China Sn province (794 °C, Xu et al., 2015). Because pressure potentially influences melting reactions and melting degree (Castro et al., 2000), two different pressures (4 vs. 7 kbar) were selected to evaluate the effects of pressure (*P*) on Sn distribution. The batch melting model was utilized in the calculation (Shaw, 1970; 1979):

$$C^L/C^0 = 1/[D + F^*(1 - D)] \qquad (1)$$

where partial melts and minerals are at chemical equilibrium, C^L is the concentration of Sn in the melt (wt.%), C^0 the concentration of Sn in the source rock (wt.%), F the weight fraction of melt produced, and D the bulk partition coefficient of Sn between residual solids and melt, namely the weighted sum of partition coefficients of Sn between individual residual phases and melt. The partition coefficients for Sn between individual minerals and melt involved in the calculation are adopted mainly from Simons et al. (2017), which were calculated by dividing mineral (from LA-ICP-MS analyses) by whole-rock Sn abundance (from ICP-MS analyses) of granites. The partition coefficient for Sn between garnet and melt was extracted from the compositions of leucocratic vein and peritectic garnet in migmatite (Zhao et al., 2022). The applicability of the reported partition coefficients for individual minerals and uncertainties introduced to thermodynamic modeling of metasediment anatexis were discussed by Zhao et al. (2022). The partition coefficient for Sn between ilmenite and silicate melt was determined experimentally at 1200 °C and 1 GPa by Klemme et al. (2006), and is taken here as an approximation in the calculation.
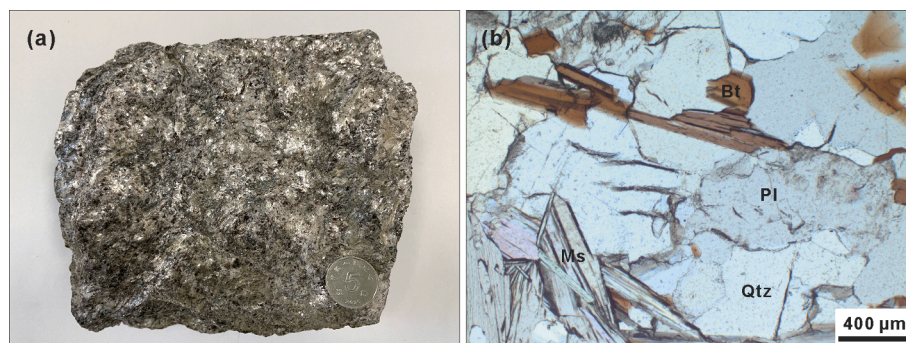

Fig. 3. Representative Mengdong mica schist sample (a) and its plane-polarized photomicrograph (b). Bt biotite, Ms muscovite, Pl plagioclase, Qtz quartz.

4. Results

4.1. Whole-rock geochemistry

The full dataset of major and trace elements for the metasediments of Mengdong, Sibao, Pingbian, and Shuangqiaoshan Groups, collected from previous works and obtained in this study, are presented in Fig. 4 and compiled in Table A1. The calculated average whole–rock compositions for the metasediments of the four groups are reported in Table 1. A brief description of the whole-rock geochemistry for these samples follows: The Mengdong mica schists contain (in wt.%) SiO_2 56.3–69.7, Al_2O_3 11.9–22.3, $Fe_2O_3^t$ 4.08–8.41, MgO 0.73–4.72, TiO_2 0.62–0.98, K_2O 1.32–5.01, Na_2O 0.22–4.65, CaO 0.01–2.49 with K_2O/(Na_2O + CaO) molar ratio 0.12–8.48, and have a high but variable Sn content with an average of 9 ppm (1σ = 5). The low-grade metasediments of Sibao Group contain (in wt.%) intermediate to high SiO_2 58.6–80.0, and Al_2O_3 11.4–20.6, $Fe_2O_3^t$ 2.75–7.83, MgO 0.47–2.87, TiO_2 0.34–0.84, K_2O 1.41–6.28, Na_2O 0.12–1.56, CaO 0.05–0.89 with K_2O/(Na_2O + CaO) between 0.50 and 14.0. The Sn content of the Sibao Group metasediments was reported from 45 samples and is on average 6.25 ppm (Mao et al., 1991). In contrast, the Pingbian metasediments have a relatively high content (in wt.%) of SiO_2 67.0–77.6, low contents of Al_2O_3 11.2–17.2, $Fe_2O_3^t$ 1.80–6.66, MgO 0.42–1.87, TiO_2 0.31–0.67, K_2O 0.23–3.82, Na_2O 0.22–5.66, and CaO 0.04–0.41 with K_2O/(Na_2O + CaO) ranging between 0.02 and 3.23. The average concentration of Sn is 5 ppm (1σ = 4). The low-grade metasediments of Shuangqiaoshan Group are composed mainly of sandstone and argillaceous rocks (low greenschist facies, Wang et al., 2014) and contain (in wt.%) SiO_2 58.4–78.7, Al_2O_3 9.50–21.3, $Fe_2O_3^t$ 1.32–9.07, MgO 0.01–2.01, TiO_2 0.54–1.07, K_2O 0.43–4.34, Na_2O 0.08–3.69, CaO 0.01–2.28, with K_2O/(Na_2O + CaO) 0.20–5.13. The Shuangqiaoshan metasediments have an average Sn concentration of 2 ppm (1σ = 1).

4.2. Thermodynamic modeling and calculation of Sn partitioning

4.2.1. P-T phase diagram

The normalized bulk compositions used for phase diagram construction are listed in Table A2. In the case of the Mengdong Group, the reported peak metamorphic conditions are 8.6 kbar and 633 °C (Tan and Liu, 2017b). At such *P-T* conditions, the predicted phase assemblages for Mengdong metasediments mainly include quartz, biotite, muscovite, plagioclase, garnet, aluminosilicate, and rutile (Fig. 5a), which agrees
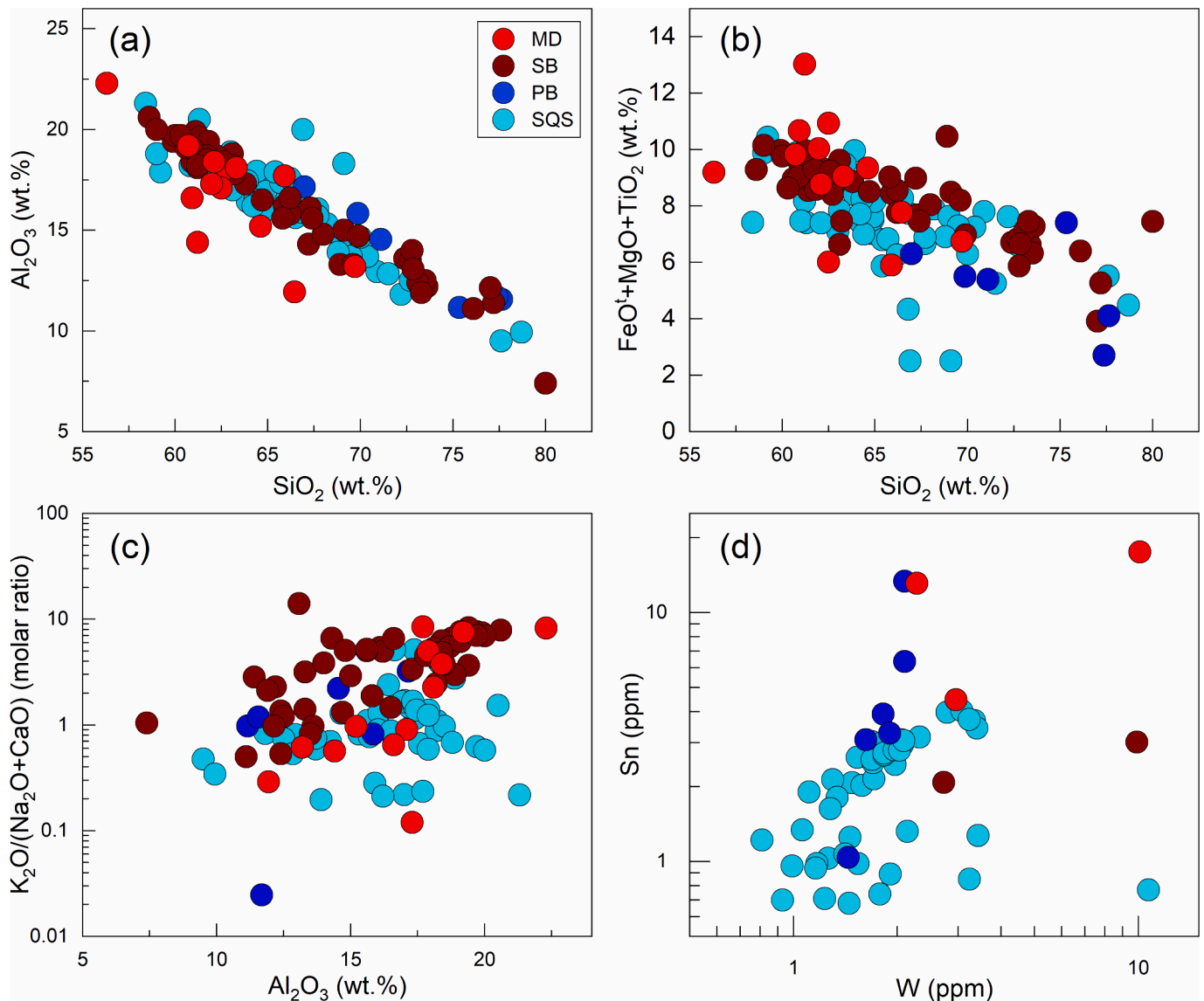

Fig. 4. Diagrams showing the geochemistry of the metasediments of Mengdong (MD), Sibao (SB), Pingbian (PB), and Shuangqiaoshan (SQS) groups. The full dataset plotted is presented in Table A1.

Table 1
Calculated average whole-rock compositions for the metasediments of the Mengdong, Sibao, Pingbian, and Shuangqiaoshan Groups in South China.

	Mengdong Group	Sibao Group	Pingbian Group	Shuangqiaoshan Group
Number of samples	13	52	6	46
wt.%				
SiO_2	62.9 (3.1)	66.2 (5.6)	73.1 (4.0)	66.0 (4.3)
$Fe_2O_3^t$	6.52 (1.37)	6.25 (1.00)	4.47 (1.52)	5.93 (1.50)
MgO	2.35 (1.12)	1.95 (0.53)	0.68 (0.17)	1.15 (0.55)
TiO_2	0.80 (0.10)	0.69 (0.12)	0.54 (0.12)	0.79 (0.13)
Al_2O_3	16.9 (2.6)	16.3 (3.0)	13.7 (2.3)	16.4 (2.5)
MnO	0.09 (0.04)	0.10 (0.03)	0.06 (0.04)	0.07 (0.05)
CaO	1.03 (0.89)	0.39 (0.17)	0.18 (0.15)	0.51 (0.39)
Na_2O	1.30 (1.20)	0.40 (0.41)	1.84 (1.82)	1.41 (0.74)
K_2O	3.47 (0.89)	3.98 (1.20)	2.24 (1.26)	2.73 (1.12)
Sn (ppm)	9 (5)	6.25	5 (4)	2 (1)

Notes: Values in parentheses are calculated standard errors (1σ) of the listed average values. Data sources: Ling and Liu, 2002; Wang et al., 2012; Wang and Zhou, 2013; Tan and Liu, 2017a; Zhou et al., 2018; Yan et al., 2019; Zhu et al., 2019; Liu et al., 2023, and this study. The full dataset is presented in Appendix Table A1. The Sn concentration of Sibao Group is adopted from Mao et al. (1991), which was reported as average from 45 samples of the Sibao Group.

with the observed phase assemblage in the studied samples. The presence of chlorite in the samples may be explained as retrograde metamorphic product of biotite. The equilibrium phase diagram shows that the solidus is located between about 678 °C and 755 °C depending on pressure. At conditions just below the solidus, the stable mineral phases mainly include quartz, biotite, muscovite, plagioclase, K-feldspar, kyanite/sillimanite, cordierite, and ilmenite (and garnet at high pressures). Biotite is stable across the range of modeled pressures at subsolidus conditions, while muscovite is stable at elevated pressures, e.g. above ~2 kbar at 600 °C. The muscovite–out curve has a positive Clapeyron slope. The lowest temperature for muscovite dehydration melting is ~678 °C at 4.7 kbar. For lower and higher pressures, the solidus temperature increases to ~750 °C at 10 kbar and 1 kbar. Above 4.7 kbar, muscovite dehydration melting is feasible only within a narrow temperature interval of ~35 °C. Muscovite melting produces less than 5 wt% melt. Incongruent melting of muscovite produces peritectic phases that mainly include biotite, K-feldspar, and sillimanite/kyanite. Compared to that of muscovite, the stability field of biotite extends to higher *PT*–conditions, e.g., 761 °C at 1.0 kbar and 845 °C at 6.9 kbar. The biotite-out curve has a negative Clapeyron slope above 6.9 kbar. Biotite dehydration melting mainly produces peritectic garnet, K-feldspar, ilmenite, rutile and orthopyroxene depending on pressure. Cordierite replaces garnet as an important peritectic phase at pressures below 6.9 kbar. Biotite dehydration melting yields a maximum of up to 25 wt% melt at 845 °C and 6.9 kbar.

The phase diagram for the metasediments of the Sibao Group is shown in Fig. 5b. The solidus depends on pressure and lies between ~683 °C (4.8 kbar) and ~755 °C (1 kbar), and ~765 °C (10 kbar). For all calculated compositions, the solidi and muscovite–out curves follow trends that are very similar to those described above for the Mengdong Group. At subsolidus conditions, the mineral assemblages mainly consist of quartz, biotite, muscovite, plagioclase, K-feldspar, kyanite/sillimanite, ilmenite, and rutile (and cordierite at pressure ≲3.3 kbar and garnet at higher pressure). Incongruent melting of muscovite starts at 683 °C and 4.8 kbar and shifts to higher temperature with pressure. The

d*P*/d*T* slope of the muscovite-out curve is steep, ~10 °C/kbar between 5 and 10 kbar. Dehydration melting of muscovite yields ~10 wt% melt between 9 and 10 kbar. At temperatures above the muscovite–out reaction, the mineral assemblages mainly include biotite, K-feldspar, plagioclase, quartz, sillimanite/kyanite, and rutile (and garnet at high pressures). The stability limit of biotite lies between 756 °C at 1.0 kbar and 858 °C at 6.7 kbar. At pressures above 6.7 kbar, the biotite-out curve has a negative Clapeyron slope. At temperatures above biotite melting, the mineral assemblages include plagioclase, K-feldspar, quartz, rutile, ilmenite, sillimanite/kyanite and orthopyroxene. Depending on pressure, garnet and/or cordierite are additionally present. Biotite dehydration melting yields up to 32 wt% melt at 858 °C and 6.7 kbar.

The modeled subsolidus assemblages of the Pingbian Group mainly include quartz, muscovite, biotite, plagioclase, K-feldspar, albite, staurolite, kyanite/sillimanite/andalusite, ilmenite, rutile and cordierite or garnet depending on pressure (Fig. 5c). In contrast to the phase diagram modeled for the Mengdong and Sibao Groups, a lower pressure limit exists for biotite at subsolidus conditions, ranging from ~1 kbar at 600 °C to ~2.5 kbar at 680 °C. Dehydration of muscovite occurs at somewhat lower temperatures of 600 °C at ~2.2 kbar. Incongruent melting of muscovite takes place within a narrow *P-T* field, which ranges between 661 °C at 4.3 kbar and 753 °C at 10 kbar. The amount of produced melt reaches a maximum of about 9 wt% at 10 kbar and the resulting mineral assemblages mainly consist of biotite, K-feldspar, plagioclase, quartz, sillimanite/kyanite, ilmenite, rutile, and garnet depending on pressure. Biotite dehydration melting occurs between ~679 °C at 2.5 kbar and 771 °C at 5.4 kbar. The biotite-out curve has a negative Clapeyron slope at pressure above 5.4 kbar. The residual mineral assemblages vary with pressure and mainly include K-feldspar, plagioclase, quartz, ilmenite, sillimanite/kyanite/andalusite, cordierite, rutile, and garnet. The amount of melt from biotite dehydration melting reaches a maximum of 14 wt% at 771 °C and 5.4 kbar.

The calculated phase diagram for the Shuangqiaoshan metasediments shows that subsolidus mineral assemblages mainly include quartz, plagioclase, muscovite, biotite, K–feldspar, kyanite/sillimanite/andalusite, ilmenite, and rutile (and cordierite at pressure below ~3.0 kbar and garnet at higher pressure) (Fig. 5d). The solidus and mica dehydration melting curves are similar to those described above for the Pingbian Group. The lowest temperature for muscovite melting is about 669 °C at 4.5 kbar and increases to ~735 °C at 1 kbar and ~753 °C at 10 kbar. Dehydration melting of muscovite is restricted to a small temperature interval of less than ~33 °C. The amount of melt generated by muscovite melting is below ~10 wt%. The mineral assemblages include mainly biotite, quartz, sillimanite, and peritectic K-feldspar and plagioclase. Biotite can be stable up to ~800 °C at 5.9 kbar and biotite dehydration melting yields at most 19 wt% melt. The residual mineral assemblages at temperatures just above the biotite-out curve can include quartz, K-feldspar, plagioclase, sillimanite, ilmenite, rutile, garnet, and cordierite depending on pressure.

4.2.2. Sn partitioning

The modeled phase assemblages and melt compositions at 800 °C, 4 kbar and 800 °C, 7 kbar for the metasediments of the four groups are reported in Tables A3 and A4. At 800 °C and 4 kbar, the mineral assemblages of the four groups include quartz, plagioclase, K-feldspar, garnet, ilmenite, cordierite and sillimanite (except for the Sibao and Mengdong Groups). In comparison, at the same temperature but at a pressure of 7 kbar, cordierite is absent in all groups, plagioclase is not predicted for the Sibao Group, and biotite is still stable in the Mengdong and Sibao Groups.

Increasing pressure from 4 to 7 kbar makes insignificant changes of the bulk partition coefficients (*D*) of Sn for the Pingbian and Shuangqiaoshan Groups (Fig. 6). By contrast, increasing pressure from 4 to 7 kbar increases *D* significantly (by ~3 to 4 times) for the Mengdong and Sibao Groups. This results from variations in the residual mineral assemblages, particularly biotite persistence. Consequently, the Sn
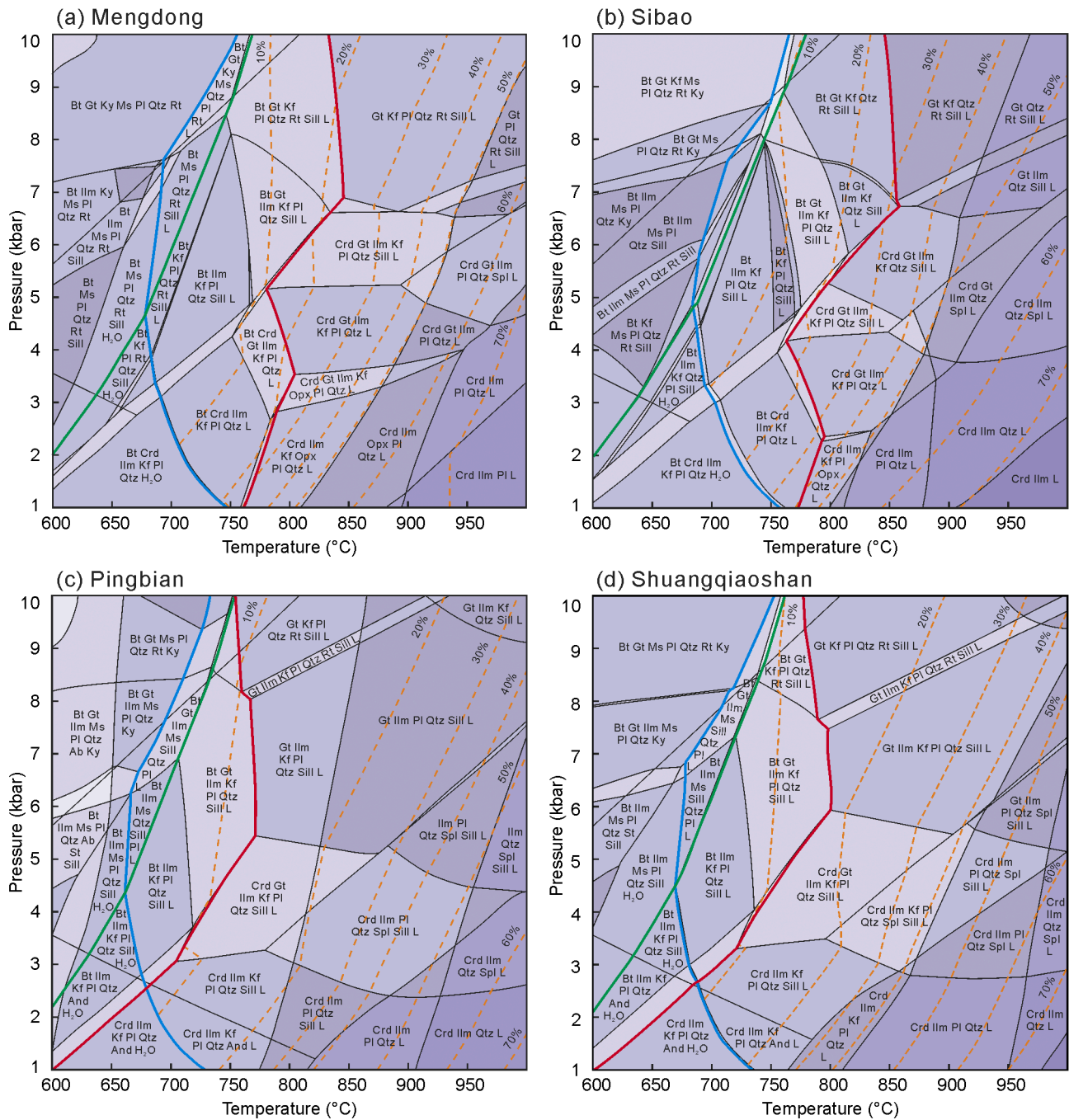
Fig. 5. Pressure–temperature (*P-T*) phase diagram calculated for the average compositions of Mengdong (a), Sibao (b), Pingbian (c), and Shuangqiaoshan (d) groups. See Appendix B for minor stability fields. The blue, green and red solid lines represent solidus, muscovite-out and biotite-out curves, respectively. The orange dash lines indicate the isopleths of melt content (wt.%) in the equilibrium phase assemblages. Abbreviations: Ab albite, And andalusite, Bt biotite, Crd cordierite, Gt garnet, Ilm ilmenite, Kf K-feldspar, Ky kyanite, L melt, Ms muscovite, Opx orthopyroxene, Pl plagioclase, Qtz quartz, Rt rutile, Sill sillimanite, Spl spinel, St staurolite.

concentrations in melt generated at 7 kbar are systematically lower for Mengdong and Sibao Groups compared to the other groups in spite of the lower melt fractions (Fig. 6). The highest Sn concentrations in melts at 4 kbar are from the Mengdong mica schist and at 7 kbar are from the Pingbian metasediments, respectively. At both pressures, the lowest Sn concentrations in melts are predicted from the Shuangqiaoshan metasediments.

5. Discussions

5.1. The exposed Precambrian metasediments as potential protolith for Sn-granites in southwest China

It has been well documented that most of the granites in South China that are associated with Sn(W) mineralization are peraluminous (Wu et al., 2017; Mao et al., 2019). The petrogenesis of highly fractionated peraluminous granites (I-, S- or even A-type) is not always uncontroversial, because their geochemistry is dictated not only by source composition but also by magmatic processes (Gao et al., 2016; 2020; Wu et al., 2017). Given the difficulty in generating large quantities of
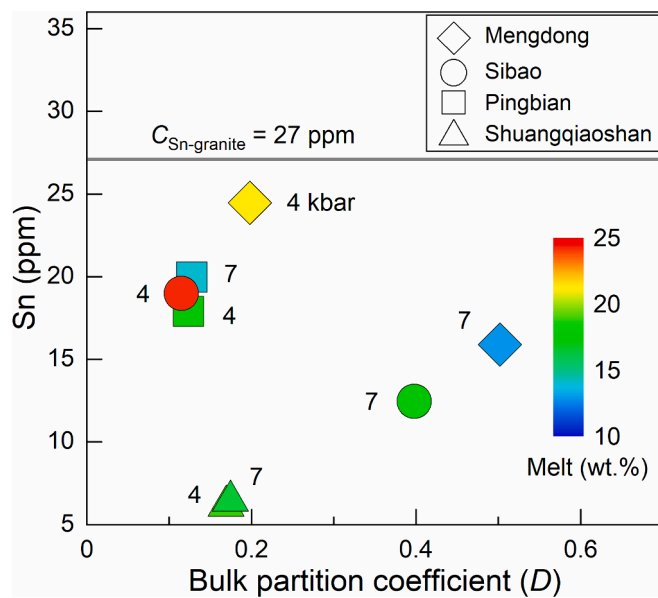
Fig. 6. Bulk Sn partition coefficients (D) between residual minerals and melt, and Sn concentrations in melts calculated for the metasediments of Mengdong, Sibao, Pingbian, and Shuangqiaoshan Groups at 800 °C, 4 kbar and 800 °C, 7 kbar. These data are presented in more detail in Tables A3 and A4. The color of the symbols depicts the mass fractions of melt in the equilibrium phase assemblages. The grey horizontal line represents the average value of Sn in the less evolved Laojunshan granites (Xu et al., 2015; Zhao et al., 2018).

peraluminous melts by removal of amphibole (diagnostic mineral for I-type granites) from metaluminous melt, the I-type scenario requires the incorporation of sedimentary components, either in a partial melt or through bulk assimilation to account for the extra alumina (Chappell et al., 2012; Wu et al., 2017) and even for ore-forming elements (Zhang et al., 2017b). In comparison, peraluminous granitic melts can be directly produced by fluid-absent melting of metasediments in the S-type model (Clements and Vielzeuf, 1987). We do not intend to fully discuss these models in the present study. Nevertheless, Sn-granites are widely believed to be generated by partial melting of metasediments (e. g., Lehmann, 1990; Romer and Kroner, 2015; 2016). The identification of the specific protolith of a Sn-granite is crucial for understanding the formation of Sn mineralization but remains a challenging task, as a granitic melt generated by partial melting may travel a considerable distance from the source (e.g., Searle et al., 2009). This can be further burdened by the poor exposure of probable protoliths. As a consequence, the protolith can often not be assigned without ambiguity. Nevertheless, the origin of Sn-enriched granitic melt has been addressed in many well-studied terrains by using geochemical and isotopic constraints (e.g., Sr-Nd and Lu-Hf isotopes) in combination with close spatial relationships between plutons and regional stratigraphy. In the Erzgebirge, for instance, detailed geochemical investigations showed repetition of early Palaeozoic metasedimentary sequences due to stacking, with the metamorphic grade of these metasediments decreasing from E to W in surface exposures (Mingram, 1998). The source of the tin granites is the same although they intruded into metasediments of different metamorphic grade (Romer and Kroner, 2015; 2016). In the case of South China, robust geochemical and isotopic evidence has been established that the Precambrian metasediments exposed in the Yangtze Block (e.g., Mengdong, Sibao, Fanjingshan, Lengjiaxi, and Shuangqiaoshan Groups) are important protoliths of the Sn- and/or W-related granites (Yu et al., 2023). The results of this study confirm that Sn concentrations in Precambrian metasediments from the southwest China are higher than those from southeast China and that the Mengdong mica schists contain the highest average concentration of Sn (Table 1). In most cases, it is assumed that Sn (and W) granites are derived from partial melting of

regional metasediments with metamorphic grades generally ranging between sub-/lower greenschist to lower amphibolite facies (e.g., met-asandstone, metapelite, slate, phyllite, schist, and gneiss). Prograde metamorphism is associated with changes in the mineral phases, abundance and composition, rock texture, and element distribution (Winter, 2013; Stepanov, 2021). It has been well documented that the major element composition of metasediments, which determines the mineralogy during prograde metamorphism, remains essentially constant until anatexis (Mingram, 1998; Hammerli et al., 2016; Stepanov, 2021; Forshaw and Pattison, 2022). Thus, the major-element compositions of metasediments reflect the geochemical characteristics of their protoliths (sediments), which variations may be associated with e.g., complex provenance. The content of trace element Sn in metasediments, however, can increase during prograde metamorphism, because Sn is fluid mobile during prograde metamorphism (Romer et al., 2022), especially if Cl and F are available as ligands (Cuney and Barbey, 2014; Schmidt, 2018). Metamorphic Sn enrichment seems plausible in the southwest China Sn province, e.g., the Laojunshan high–grade metamorphic complex (Liu et al., 2021). This region is the intersection of several blocks and experienced multistage intense metamorphism (Wang et al., 2020 and references therein), in contrast to the Jiangnan Orogen where low-grade metasediments are predominant (Wang et al., 2014). For the Mengdong mica schist and unexposed analogues in that area, prograde metamorphism could have led to the enrichment of Sn by fluid mobilization, although additional introduction by the emplacement of Laojunshan granites cannot be eliminated. It is important to bear in mind that the stratiform-like skarn in the Mengdong Group hosts the giant Nanyangtian W deposit and bears the characteristics of multiple stages of structural deformation and mineralization, which are older than the Laojunshan granites (Zhang et al., 2021 and references therein). The Sn contents of the Mengdong mica schists from the surrounding area can locally reach more than 60 ppm (Que, 2016). Furthermore, it was proposed that the Xinzhai Sn deposit (Fig. 2) where cassiterite-schist type (cassiterite ores hosted by schist) is one of the most developed types of Sn mineralization, resulted from metamorphic mobilization of Sn from the Precambrian schists (Cambrian in some older literature) (Wang, 1994; Zhang et al., 2021 and references therein).

5.2. Role of protolith composition in generation of Sn-fertile granitic melts

In the following, we relate geochemical characteristics of the Precambrian metasediments from South China to the formation of Sn-bearing granitic melts. We first discuss the major element composition of the metasediments as a first proxy for the generation of Sn–enriched granitic melts, because this composition controls the onset of melting, melt productivity and melting reactions. Secondly, we discuss the Sn–content of the metasediments with respect to the formation of Sn–enriched granitic melts in southwest China.

Phase equilibria modeling reveals that the reaction boundaries, such as the solidi, are generally similar among the four compositions (Mengdong, Sibao, Pingbian, and Shuangqiaoshan Groups), ranging from 661–683 °C at 4.3–4.8 kbar to 733–765 °C at 10 kbar (Fig. 5). Muscovite melting occurs within a narrow temperature interval of less than 35 °C and <10 wt% melt is generated by dehydration melting of muscovite. The obtained phase diagrams for metasediments of the Mengdong and Sibao Groups show similar topologies, as is readily noticed, for example, from the locations of the solidus and of the biotite-out curve (Fig. 5a and 5b). The amount of melt generated during incongruent biotite melting varies depending on temperature and pressure, and reaches a maximum of 25 wt% at 845 °C and 6.9 kbar for the Mengdong Group, and 33 wt% at 858 °C and 6.7 kbar for the Sibao Group. Among the investigated samples, the Pingbian metasediments have the highest silica and the lowest Al_2O_3, $Fe_2O_3^t$, MgO, and TiO_2 contents due to the high proportion of siliceous components (e.g., quartz, feldspar). This compositional variation greatly affects, for

instance, the biotite-out curve, which is located at lower temperatures compared to those of the Mengdong and Sibao Groups (Fig. 5). For the Pingbian Group, the highest amount of melt (14 wt%) is expected to form at 771 °C and 5.4 kbar. The phase diagram topologies for the Shuangqiaoshan and Pingbian Groups are similar (Fig. 5d), although the SiO_2, Al_2O_3, $Fe_2O_3^t$, MgO, and TiO_2 contents of the Shuangqiaoshan Group are much closer to those of the Sibao and Mengdong Groups (Table 1). It is worth noting that the Pingbian and Shuangqiaoshan metasediments have a lower K_2O content and a higher Na_2O content compared with the Mengdong and Sibao Groups. In the case of the Shuangqiaoshan Group, up to ~19 wt% melt can be generated at 800 °C and 5.9 kbar. Compared with the Mengdong and Sibao Groups, the relatively low melt fertility of the Pingbian and Shuangqiaoshan Groups in terms of dehydration melting of biotite can be explained by the difference in major-element composition: low Na_2O and high K_2O, $Fe_2O_3^t$, MgO, TiO_2 contents results in a high proportion of biotite in the metasediments during subsolidus prograde metamorphism. Consequently, a high amount of melt is produced by biotite dehydration melting. It should be noted that quartz and alkali feldspar are essential components of granitic melts and an excess of refractory components ($Fe_2O_3^t$, MgO, TiO_2, Al_2O_3) will result in a rather infertile source (Patiño Douce and Johnston, 1991). This indicates that the initial protolith composition, controlled by the proportion of siliceous and argillaceous components, is an important parameter for melt production by fluid-absent melting of micas. Rocks of psammitic derivation, e.g., clay-rich metasandstones, may be fertile protoliths during crustal anatexis (Patiño Douce and Johnston, 1991; Montel and Vielzeuf, 1997).

According to our modeling, all four samples produce melts that are peraluminous and felsic in composition at both 800 °C, 4 kbar and 800 °C, 7 kbar (Table A4). The bulk partition coefficients of Sn for all samples are similar at 4 kbar, but vary significantly at 7 kbar due to the various stabilities of Sn-sequestering minerals, especially biotite (Fig. 6; Table A3). Ilmenite and tourmaline exert insignificant influence on the bulk *D* for Sn in comparison with biotite, though both have the potential to host high amounts of Sn. This is due to the low abundances of ilmenite and tourmaline in the equilibrium phase assemblages. Other accessory minerals such as apatite and zircon, which are observed in the sampled mica schists, host very little Sn. Cordierite and garnet are not Sn-sequestering phases and their presence during partial melting does not contribute to the increase of the bulk *D* for Sn. Despite the higher bulk mineral-melt partition coefficients of Sn at 4 kbar, the anatectic melts of the Mengdong mica schists are expected to be highest in Sn among the four Groups (Fig. 6). The lowest Sn contents at both 4 and 7 kbar are expected for melts from the Shuangqiaoshan metasediments. This can be attributed to the initial Sn concentration: the average Sn in the Mengdong metasediments (9 ppm) is nearly 1.5 times higher than that in the Sibao Group (6.25 ppm), nearly twofold enriched relative to the Pingbian Group (5 ppm), and more than four times as high as in the Shuangqiaoshan Group (2 ppm). The Sn contents in the melts for the Mengdong and Sibao Groups at 7 kbar are lower than those for the Pingbian Group due to their further enhanced bulk mineral-melt *D* of Sn. In comparison, Sn granites contain 16–30 ppm Sn (Lehmann, 2021). In the case of Laojunshan Sn granites in southwest China (Fig. 2), the Sn contents of the less evolved granites are reported to be in the range of 20–37 ppm (Xu et al., 2015; Zhao et al., 2018). Assuming the anatectic temperature of metasediments for the generation of Laojunshan granites is 800 °C (the highest zircon saturation temperature for the less evolved Laojunshan granites is 794 °C, Xu et al., 2015), the calculated Sn contents in the melts for the Mengdong Group at 4 and 7 kbar are 24.5 ppm (melt fraction 21.1 wt%) and 15.9 ppm (12.9 wt%), respectively. These concentrations are very close to those in the Laojunshan granites (Fig. 6). Therefore, the Mengdong group is the most likely source of Sn–enriched granitic melt in the Dulong Sn district, southwest China (Fig. 2). By contrast, the Sn contents in the melts for the Shuangqiaoshan metasediments at 4 and 7 kbar are with 6 ppm significantly lower than in granitic melts associated with the formation of Sn–deposits. It should

be kept in mind that Sn contents in granites related to Sn mineralization are mostly above 10 ppm (Fig. 6 in Lehmann, 2021). This supports the hypothesis that pre-enrichment of Sn in the source rocks and melting reactions make the formation of Sn-enriched granitic melts during anatexis particularly efficient (Romer and Kroner, 2015; 2016; 2022).

5.3. Implications for the formation of Sn-enriched granites

We demonstrate the role of major element composition and Sn content in metasediments for the formation of Sn–enriched granites. Although we focus on South China, our results may be applicable to worldwide Sn–enriched granites.

One factor affecting melt composition during partial melting is the metamorphic phase assemblage, which is controlled by the bulk major element compositions (Fig. 5; Tables A3 and A4). The stability of Sn-hosting phases (e.g. biotite, rutile) affects the bulk Sn partition coefficient and consequently controls the release of Sn into the granitic melt. Our results suggest that particularly the content of biotite affects the bulk distribution coefficient of Sn significantly. The stability of accessory minerals that can be important host phases for Sn, such as Fe–Ti–oxides, are also a function of whole-rock composition, next to temperature and pressure (Meinhold, 2010). In the cases of the Mengdong and Sibao samples, rutile becomes stable at low-pressure conditions even before the onset of melting (Fig. 5a and 5b). In contrast, in the Pingbian and Shuangqiaoshan Groups, rutile stability is restricted to higher pressures (Fig. 5c and 5d). Accordingly, ilmenite occurs mainly in the stability fields above the solidus and at pressures below ~ 7–8 kbar in the phase diagrams of the Mengdong and Sibao Groups (Fig. 5a and b). In the case of the Pingbian and Shuangqiaoshan Groups, ilmenite is stable across the modeled *P-T* conditions except for small fields at higher pressures (above ~ 7–8 kbar) (Fig. 5c and d). Regarding melt production, relatively high degrees of melting before the complete consumption of biotite are favorable for the connection and migration of Sn-enriched melts from the residual solids (Daines and Pec, 2015). Based on this, clay-rich feldspathic metasandstones or mica schists are probably favorable source rocks for Sn (and W) granites, given their high modal abundances of micas due to their capacity to host significant amounts of Sn (and W) and their fertility in producing melts (Patiño Douce and Johnston, 1991).

In combination with the degree of melting, another crucial aspect on the formation of Sn–enriched melts is the Sn concentration in the metasediments, as indicated by the calculated results (Fig. 6). Fertile source rocks allow high-degree partial melting to produce Sn–enriched melts, whereas similar Sn concentrations in melts derived from an average protolith are only feasible by low-degree partial melting. Fertile protoliths for Sn and/or W granites can result from prograde metamorphism of (meta–) sediments and can result from chemical weathering and redistribution of weathered sediments (Romer and Kroner, 2015; 2016).

In the case of South China, we show that the Sn contents in main metasediments from the southwest China Sn province (Sibao, Mengdong, and Pingbian Groups) are higher than those of main metasediments from the southeast China W province (Shuangqiaoshan Group) (Table 1). No systematic variation in Sn contents among the Precambrian metasediments from southeast to southwest China along the Jiangnan Orogenic belt can be demonstrated (Fig. 6a in Yu et al., 2023). Noticeably, it was reported that the unaltered metasediments of the Shuangqiaoshan Group from the periphery of the W-mineralized area have average contents of 21 ppm Sn and 12 ppm W (Liu et al., 1983). That is, the Sn concentrations in the metasediments are about the same level as those of Sn-enriched granites in the same area. Recently, zircon Hf isotopic mapping using data of main Mesozoic granitoids and silicic volcanic rocks in South China revealed that the crust in South China is isotopically heterogeneous (Zhang et al., 2023).

We propose that, apart from melting temperature and melting reaction, the heterogeneous distribution of pre-enriched favorable source rocks, regionally and locally (e.g., sediment packages) has contributed

to the spatial distribution of major Sn and W districts in South China as well as other regions worldwide. For instance, in the Erzgebirge Sn province (Central Europe), a striking and significant regional crustal Sn anomaly exists in the form of stratiform cassiterite mineralization in the Schwarzenberg-Aue district, which likely resulted from pre-magmatic sedimentary and/or metamorphic processes (Romer et al., 2022; Weber et al., 2023). This model can explain why highly evolved Sn and W infertile granites, with a magmatic evolution comparable to mineralized Sn and W granites, are present within the same metallogenic belts. As another example, the economically most important W mineralization in North American Cordillera is restricted to the narrow Canadian W Belt, where the melt extraction temperatures are consistently above 800 °C based on zircon saturation thermometry, and W mineralization is specifically associated with the pre-enriched metasediments (Elongo et al., 2022). Source control on the genesis of granite-related Sn deposits may further be the case for the Southeast Asian Sn belt, the Appalachian-Variscan orogenetic belt, South America Sn belt, and other regions worldwide (Cobbing, 1990; Romer and Kroner, 2016, 2022; Yang et al., 2020).

Fractional crystallization may be one but certainly not the only important process in the formation of Sn deposits. For example, for the interpretation of the isotopic evidence Carr et al. (2021) had to combine fractional crystallization of a melt derived from a basaltic source with assimilation of Ordovician sediments to explain the enrichment of tin in the final melt. In contrast to our hypothesis, the fractional crystallization model (e.g., Lehmann, 2021) cannot explain why highly evolved granites do not always show enhanced Sn contents, whereas Sn enrichment can occur in granites with less extreme fractionation. If fractional crystallization would be the main process controlling magmatic Sn enrichment, tin granites would not occur just in a few provinces. In Mongolia, there are few and rather small Sn deposits although often very fractionated anorogenic granites are abundant. For example, Ongon-Khairkhan in central Mongolia, is the type locality of ongonite, a highly fractionated topaz-bearing microleucogranite enriched in Sn (30–43 ppm), W (4–10 ppm), Rb, Cs, Nb, Ta and F. A tungsten deposit is spatially associated, but there is no Sn deposit (Dostal et al., 2015). Moreover, almost all tin deposits have ages that are younger than the start of modern-style subduction, thus processes other than fractional crystallization are involved in the formation of Sn deposits.

6. Conclusions

The here presented thermodynamic modeling demonstrates the significant role of protolith composition for the formation of Sn-enriched granitic melts. On one hand, the major element composition of metasediments mainly determines the melting reaction, mineralogy of restite and melt productivity at specific anatectic conditions, e.g., high–temperature melting (800 °C), and therefore controls the partition behavior of Sn (and W) during partial melting. On the other hand, the concentration of Sn (and W) in the source rocks, resulting from metamorphic fluid mobilization and/or intense chemical weathering, profoundly affect the fertility of anatectic melt. We propose that the distribution of favorable source rocks has contributed to controlling the spatial distribution of Sn (and W) mineralization. The distribution of such favorable source rocks might be heterogeneous in South China and other major Sn and W districts worldwide.

Declaration of competing interest

The authors declare that they have no known competing financial interests or personal relationships that could have appeared to influence the work reported in this paper.

Data availability

Data will be made available on request.

Appendix A. Supplementary data

Supplementary data to this article can be found online at https://doi.org/10.1016/j.oregeorev.2024.106094.

References

Carr, P., Norman, M.D., Bennett, V.C., Blevin, P.L., 2021. Tin enrichment in magmatic-hydrothermal environments associated with cassiterite mineralization at Ardlethan, Eastern Australia: Insights from Rb-Sr and Sm-Nd isotope compositions in tourmaline. Econ. Geol. 116, 147–167.

Castro, A., Guillermo Corretgé, L., El-Biad, M., El-Hmidi, H., Fernández, C., Patiño Douce, A.E., 2000. Experimental constraints on Hercynian anatexis in the Iberian Massif, Spain. J. Petrol. 41, 1471–1488.

Chappell, B.W., Bryant, C.J., Wyborn, D., 2012. Peraluminous I-type granites. Lithos 153, 142–153.

Chen, X.C., Hu, R.Z., Bi, X.W., Zhong, H., Lan, J.B., Zhao, C.H., Zhu, J.J., 2015. Zircon U-Pb ages and Hf-O isotopes, and whole-rock Sr-Nd isotopes of the Bozhushan granite, Yunnan province, SW China: Constraints on petrogenesis and tectonic setting. J. Asian Earth Sci. 99, 57–71.

Cheng, Y.B., Mao, J.W., 2010. Ages and geochemistry of granites in Gejiu area, Yunnan province, SW China: Constrains on their petrogenesis and tectonic setting. Lithos 120, 258–276.

Cheng, Y.B., Mao, J.W., Liu, P., 2016. Geodynamic setting of Late Cretaceous Sn-W mineralization in southeastern Yunnan and northeastern Vietnam. Solid Earth Sci. 1, 79–88.

Clements, J.D., Vielzeuf, D., 1987. Constraints on melting and magma production in the crust. Earth Planet. Sci. Lett. 86, 287–306.

Cobbing, J., 1990. A comparison of granites and their tectonic settings from the South American Andes and the Southeast Asian tin belt. GSA Special Papers 214, 193–204.

Cuney, M., Barbey, P., 2014. Uranium, rare metals, and granulite-facies metamorphism. Geosci. Front. 5, 729–745.

Daines, M.J., Pec, M., 2015, Migration of Melt. In: The Encyclopedia of Volcanoes (Second Edition) (ed Sigurdsson H). Academic Press, 49–64.

Dostal, J., Kontak, D., Gerel, O., Shellnutt, J.G., Fayek, M., 2015. Cretaceous ongonites (topaz-bearing albite-rich microleucogranites) from Ongon Khairkhan, Central Mongolia: Products of extreme magmatic fractionation and pervasive metasomatic fluid: Rock interaction. Lithos 236–237, 173–189.

Elongo, V., Falck, H., Rasmussen, K.L., Robbins, L.J., Creaser, R.A., Luo, Y., Pearson, D.G., Sarkar, C., Adlakha, E., Palmer, M.C., Scott, J.M., Hickey, K., Konhauser, K., Lecumberri-Sanchez, P., 2022. Ancient roots of tungsten in western North America. Geology 50, 791–795.

Forshaw, J.B., Pattison, D.R.M., 2022. Major-element geochemistry of pelites. Geology 51, 39–43.

Fuhrman, M.L., Lindsley, D.H., 1988. Ternary-feldspar modeling and thermometry. Am. Mineral. 73, 201–215.

Gao, P., Zheng, Y.F., Zhao, Z.F., 2016. Distinction between S-type and peraluminous I-type granites: Zircon versus whole-rock geochemistry. Lithos 258–259, 77–91.

Gao, P., Garcia-Arias, M., Chen, Y.X., Zhao, Z.F., 2020. Origin of peraluminous A-type granites from appropriate sources at moderate to low pressures and high temperatures. Lithos 352–353, 105287.

Garcia-Arias, M., Stevens, G., 2017. Phase equilibrium modelling of granite magma petrogenesis: A. An evaluation of the magma compositions produced by crystal entrainment in the source. Lithos 277, 131–153.

Guo, J., Wu, K., Seltmann, R., Zhang, R.Q., Ling, M.X., Li, C.Y., Sun, W.D., 2022. Unraveling the link between mantle upwelling and formation of Sn-bearing granitic rocks in the world-class Dachang tin district, South China. GSA Bull. 134, 1043–1064.

Hammerli, J., Spandler, C., Oliver, N.H.S., 2016. Element redistribution and mobility during upper crustal metamorphism of metasedimentary rocks: An example from the eastern Mount Lofty Ranges, South Australia. Contrib. Mineral. Petrol. 171, 36.

Han, Z.D., Golev, V., Edraki, M., 2021. A review of tungsten resources and potential extraction from mine waste. Minerals 11, 701.

Heinrich, C.A., 1990. The chemistry of hydrothermal tin (-tungsten) ore deposition. Econ. Geol. 85, 457–481.

Holland, T.J.B., Powell, R., 2011. An improved and extended internally consistent thermodynamic dataset for phases of petrological interest, involving a new equation of state for solids. J. Metamorphic Geol. 29, 333–383.

Ishihara, S., 1977. The magnetite-series and ilmenite-series granitic rocks. Min. Geol. 27, 293–305.

Ishihara, S., 1981. The granitoid series and mineralization. Econ. Geol. 75, 458–484.

Johnson, T., Brown, M., 2004. Quantitative constraints on metamorphism in the Variscides of southern Brittany—a complementary pseudosection approach. J. Petrol. 45, 1237–1259.

Klemme, S., Günther, D., Hametner, K., Prowatke, S., Zack, T., 2006. The partitioning of trace elements between ilmenite, ulvospinel, armalcolite and silicate melts with implications for the early differentiation of the moon. Chem. Geol. 234, 251–263.

Korges, M., Weis, P., Lüders, V., Laurent, O., 2018. Depressurization and boiling of a single magmatic fluid as a mechanism for tin-tungsten deposit formation. Geology 46, 75–78.

Lehmann, B., 1990. Metallogeny of tin. Springer, Berlin, p. 211 p..

Lehmann, B., 2021. Formation of tin ore deposits: A reassessment. Lithos 402–403, 105756.

Li, Q.L., Lin, W., Wang, Y., Faure, M., Meng, L.T., Wang, H., Van Nguyen, V., Thu, H.L.T., Lepvrier, C., Chu, Y., Wei, W., 2021. Detrital zircon U-Pb age distributions and Hf isotopic constraints of the Ailaoshan-Song Ma Suture Zone and their paleogeographic implications for the Eastern Paleo-Tethys evolution. Earth-Sci. Rev. 221, 103789.

Ling, Q.C., Liu, C.Q., 2002. Geochemical behavior of trace element during hydrothermal alteration in low-metamorphic rocks: A case study for Shuangqiaoshan Group in Yinshan area, northwestern Jiangxi province, China. Acta Petrologica Sinica 18, 100–108 in Chinese with English abstract.

Liu, Z., Cao, S.Y., Dong, Y.L., Li, W., Cheng, X.M., Wang, H.B., Lyu, M., 2021. Deformation structure and exhumation process of the Laojunshan gneiss dome in southeastern Yunnan of China. Sci. China Earth Sci. 64, 2190–2216.

Liu, Y.J., Li, Z.L., Ma, D.S., 1983. Studies on geochemistry of tungsten-bearing formations in South China. Scientia Sinica (Series B) 26, 396–412.

Liu, Y.P., Li, C.Y., Gu, T., Wang, J.L., 2000. Lead isotopic characteristics and age assignment of moderate to high-grade metamorphic rock series in Laojunshan, southeastern Yunnan. Acta Mineralogica Sinica 20, 228–232 in Chinese with English abstract.

Liu, B.Q., Yu, J.H., Jiang, W., Cai, Y.F., 2023. Geochemistry of the meta-sedimentary rocks of the Shuangqiaoshan Group and their genetic link to tungsten mineralization in northern Jiangxi, South China. Acta Geologica Sinica 97, 433–447 in Chinese with English abstract.

Liu, Y.B., Zhang, L.F., Mo, X.X., Santosh, M., Dong, G.C., Zhou, H.Y., 2020. The giant tin polymetallic mineralization in southwest China: Integrated geochemical and isotopic constraints and implications for Cretaceous tectonomagmatic event. Geosci. Front. 11, 1593–1608.

Mao, J.W., Lehmann, B., Schneider, H.-J., 1991. Preliminary enrichment of tin in the earth and its relationship to metallogenesis of tin deposits. J. Hebei College Geol. 14, 46–60 in Chinese with English abstract.

Mao, J.W., Cheng, Y.B., Chen, M.H., Pirajno, F., 2013. Major types and time-space distribution of Mesozoic ore deposits in South China and their geodynamic settings. Mineralium Deposita 48, 267–294.

Mao, J.W., Ouyang, H.G., Song, S.W., Santosh, M., Yuan, S.D., Zhou, Z.H., Zheng, W., Liu, H., Liu, P., Cheng, Y.B., Chen, M.H., 2019. Geology and metallogeny of tungsten and tin deposits in China. SEG Special Publications 22, 411–482.

Meinhold, G., 2010. Rutile and its applications in earth sciences. Earth-Sci. Rev. 102, 1–28.

Mingram, B., 1998. The Erzgebirge, Germany, a subducted part of northern Gondwana: Geochemical evidence for repetition of early Palaeozoic metasedimentary sequences in metamorphic thrust units. Geol. Magaz. 135, 785–801.

Montel, J.-M., Vielzeuf, D., 1997. Partial melting of metagreywackes, Part II. Compositions of mineral and melts. Contrib. Mineral. Petrol. 128, 176–196.

Palin, R.M., Weller, O.M., Waters, D.J., Dyck, B., 2016. Quantifying geological uncertainty in metamorphic phase equilibria modelling: A Monte Carlo assessment and implications for tectonic interpretations. Geosci. Front. 7, 591–607.

Patiño Douce, A.E., Johnston, A.D., 1991. Phase equilibria and melt productivity in the pelitic system: Implications for the origin of peraluminous granitoids and aluminous granulites. Contrib. Mineral. Petrol. 107, 202–218.

Que, C.Y. 2016, Tungsten metallogenic system and prospecting direction in the Nanwenhe-Saxi area, Malipo county, Yunnan Province. PhD thesis, Beijing, China, China University of Geosciences (Beijing), 220 p. (in Chinese with English abstract).

Romer, R.L., Pichavant, M., 2021, Rare metal (Sn, W, Ta-Nb, Li) granites and pegmatites, *in* Alderton, D., and Elias, S.A., eds., Encyclopedia of Geology, 2nd ed.: Elsevier, p. 840–846.

Romer, R.L., Kroner, U., 2015. Sediment and weathering control on the distribution of Paleozoic magmatic tin-tungsten mineralization. Mineral. Deposita 50, 327–338.

Romer, R.L., Kroner, U., 2016. Phanerozoic tin and tungsten mineralization—Tectonic controls on the distribution of enriched protoliths and heat sources for crustal melting. Gondwana Res. 31, 60–95.

Romer, R.L., Kroner, U., 2022. Provenance control on the distribution of endogenic Sn-W, Au, and U mineralization within the Gondwana-Laurussia plate boundary zone. Geol. Soc. Am. Special Paper 554.

Romer, R.L., Kroner, U., Schmidt, C., Legler, C., 2022. Mobilization of tin during continental subduction-accretion processes. Geology 50, 1361–1365.

Schmidt, C., 2018. Formation of hydrothermal tin deposits: Raman spectroscopic evidence for an important role of aqueous Sn(IV) species. Geochimica Et Cosmochimica Acta 220, 499–511.

Schmidt, C., Romer, R.L., Wohlgemuth-Ueberwasser, C.C., Appelt, O., 2020. Partitioning of Sn and W between granitic melt and aqueous fluids. Ore Geol. Rev. 117, 103263.

Searle, M.P., Cottle, J.M., Streule, M.J., Waters, D.J., 2009. Crustal melt granites and migmatites along the Himalaya: Melt source, segregation, transport and granite

emplacement mechanisms. Earth Environ. Sci. Trans. Royal Soc. Edinburgh 100, 219–233.

Shaw, D.M., 1970. Trace element fractionation during anatexis. Geochimica Et Cosmochimica Acta 34, 237–243.

Shaw, D.M., 1979. Trace element melting models. Phys. Chem. Earth 11, 577–586.

Simons, B., Andersen, J.C.Ø., Shail, R.K., Jenner, F.E., 2017. Fractionation of Li, Be, Ga, Nb, Ta, In, Sn, Sb, W and Bi in the peraluminous Early Permian Variscan granites of the Cornubian Batholith: Precursor processes to magmatic-hydrothermal mineralization. Lithos 278–281, 491–512.

Song, S.W., Mao, J.W., Yuan, S.D., Jian, W., 2022. Decoupling of Sn and W mineralization in a highly fractionated reduced granitic magma province: A case study from the Youjiang basin and Jiangnan tungsten belt. Mineralium Deposita 57, 1251–1267.

Stepanov, A.S., 2021. A review of the geochemical changes occurring during metamorphic devolatilization of metasedimentary rocks. Chem. Geol. 568, 120080.

Tan, H.Q., Liu, Y.P., 2017a. Tectonic setting of the Mengdong Group complex, southeast Yunnan Province: Geochemical constraints from metasedimentary rocks. Acta Geologica Sinica 61, 1416–1432 in Chinese with English abstract.

Tan, H.Q., Liu, Y.P., 2017b. Metamorphic and deformation of the Mengdong Group complex in southeast Yunnan Province and their tectonic implications. Acta Geologica Sinica 91, 15–42 in Chinese with English abstract.

Taylor, J.R., Wall, V.J., 1992. The behavior of tin in granitoid magmas. Econ. Geol. 87, 403–420.

USGS, 2023, Mineral commodity summaries 2023. U.S. Geological Survey, 210 p.

Wang, X.K., 1994. Geological-geochemical characteristics of Xinzhai tin deposit in Malipo. Yunnan Geol. 13, 1–16 in Chinese with English abstract.

Wang, Q.F., Yang, L., Xu, X.J., Santosh, M., Wang, Y.N., Wang, T.Y., Chen, F.G., Wang, R. X., Gao, L., Liu, X.F., Yang, S.J., Zeng, Y.S., Chen, J.H., Zhang, Q.Z., Deng, J., 2020. Multi-stage tectonics and metallogeny associated with Phanerozoic evolution of the South China Block: A holistic perspective from the Youjiang Bain. Earth-Sci. Rev. 211, 103405.

Wang, W., Zhou, M.F., Yan, D.P., Li, J.W., 2012. Depositional age, provenance, and tectonic setting of the Neoproterozoic Sibao Group, southeastern Yangtze Block, South China. Precambr. Res. 192–195, 107–124.

Wang, W., Zhou, M.F., 2013. Petrological and geological constraints on provenance, paleoweathering, and tectonic setting of the Neoproterozoic sedimentary basin in the eastern Jiangnan orogen, South China. J. Sediment. Res. 83, 975–994.

Wang, X.L., Zhou, J.C., Griffin, W.L., Zhao, G.C., Yu, J.H., Qiu, J.S., Zhang, Y.J., Xing, G. F., 2014. Geochemical zonation across a Neoproterozoic orogenic belt: Isotopic evidence from granitoids and metasedimentary rocks of the Jiangnan orogen, China. Precambr. Res. 242, 154–171.

Weber, S., Legler, C., Kallmeier, E., Schulz, B., Burisch, M., 2023. Metamorphic origin of stratiform cassiterite mineralization in the Schwarzenberg-Aue district–Clues to the metamorphic history and pre-orogenic Sn enrichment of the Erzgebirge (Germany). Lithos 454–455, 107273.

White, R.W., Powell, R., Holland, T.J.B., Worley, B.A., 2000. The effect of TiO₂ and Fe₂O₃ on metapelitic assemblages at greenschist and amphibolite facies conditions: Mineral equilibria calculations in the system K₂O-FeO-MgO-Al₂O₃-SiO₂-H₂O-TiO₂-Fe₂O₃. J. Metamorphic Geol. 18, 497–511.

White, R.W., Powell, R., Clarke, G.L., 2002. The interpretation of reaction textures in Fe-rich metapelitic granulites of the Musgrave block, Central Australia: Constraints from mineral equilibria calculations in the system. J. Metamorphic Geol. 20, 41–55.

White, R.W., Powell, R., Holland, T., Johnson, T., Green, E., 2014. New mineral activity-composition relations for thermodynamic calculations in metapelitic systems. J. Metamorphic Geol. 32, 261–286.

Winter, J.D., 2013. In: Principles of igneous and metamorphic petrology, 2nd ed. Pearson Prentice Hall, New York, p. 738 p..

Wolf, M., Romer, R.L., Franz, L., López-Moro, F.J., 2018. Tin in granitic melts: The role of melting temperature and protolith composition. Lithos 310–311, 20–30.

Wu, F.Y., Liu, X.C., Ji, W.Q., Wang, J.M., Yang, L., 2017. Highly fractionated granites: Recognition and research. Sci. China Earth Sci. 60, 1201–1219.

Xiang, H., Connolly, J.A.D., 2021. GeoPS: An interactive visual computing tool for thermodynamic modelling of phase equilibria. J. Metamorphic Geol. 40, 243–255.

Xu, B., Jiang, S.Y., Wang, R., Ma, L., Zhao, K.D., Yan, X., 2015. Late Cretaceous granites from the giant Dulong Sn-polymetallic ore district in Yunnan Province, South China: Geochronology, geochemistry, mineral chemistry and Nd-Hf isotopic compositions. Lithos 218–219, 54–72.

Yan, C.L., Shu, L.S., Faure, M., Chen, Y., Huang, R.B., 2019. Time constraints on the closure of the Paleo-South China Ocean and the Neoproterozoic assembly of the Yangtze and Cathaysia blocks: Insight from new detrital zircon analyses. Gondwana Res. 73, 175–189.

Yang, C.R., Tan, Q.Y., Zeng, X.L., Zhang, Y.P., Wang, Z.S., Li, J.H., 2018. Measuring the sustainability of tin in China. Sci. Total Environ. 635, 1351–1359.

Yang, J.H., Zhou, M.F., Hu, R.Z., Zhong, H., Williams-Jones, A.E., Liu, L., Zhang, X.C., Fu, Y.Z., Mao, W., 2020. Granite-related tin metallogenic events and key controlling factors in Peninsular Malaysia, Southeast Asia: New insights from cassiterite U-Pb dating and zircon geochemistry. Econ. Geol. 115, 581–601.

Yu, J.H., Cai, Y.F., Sun, T., Jiang, W., Zhang, R.Q., Griffin, W.L., Mao, Z.Q., Xia, L., 2023. Distribution and enrichment of rare metal elements in the basement rocks of South China: Controls on rare-metal mineralization. Ore Geol. Rev. 163, 105797.

Yuan, S.D., Williams-Jones, A.E., Romer, R.L., Zhao, P.L., Mao, J.W., 2019. Protolith-related thermal controls on the decoupling of Sn and W in Sn-W metallogenic provinces: Insights from the Nanling region, China. Econ. Geol. 17, 13–54.

Zhang, Z.Y., Hou, Z.Q., Lv, Q.T., Zhang, X.W., Pan, X.F., Fan, X.K., Zhang, Y.Q., Wang, C. G., Lv, Y.J., 2023. Crustal architectural controls on critical metal ore systems in South China based on Hf isotopic mapping. Geology 51, 738–742.

Zhang, R.Q., Lu, J.J., Lehmann, B., Li, C.Y., Li, G.L., Zhang, L.P., Guo, J., Sun, W.D., 2017a. Combined zircon and cassiterite U-Pb dating of the Piaotang granite-related tungsten–tin deposit, southern Jiangxi tungsten district, China. Ore Geol. Rev. 82, 268–284.

Zhang, Y., Yang, J.H., Chen, J.Y., Wang, H., Xiang, Y.X., 2017b. Petrogenesis of Jurassic tungsten-bearing granites in the Nanling Range, South China: Evidence from whole-rock geochemistry and zircon U-Pb and Hf-O isotopes. Lithos 278–281, 166–180.

Zhang, X.M., Zhang, D., Bi, M.F., Wu, G.G., Fan, Z.Z., Que, C.Y., Di, Y.J., Xue, W., Zhou, Z.G., Bai, H., 2021. Genesis and geodynamic setting of the Nanyangtian tungsten deposit, SW China: Constraints from structural deformation, geochronology, and S-O isotope data. Ore Geol. Rev. 138, 104354.

Zhao, Z.Y., Hou, L., Ding, J., Zhang, Q.M., Wu, S.Y., 2018. A genetic link between Late Cretaceous granitic magmatism and Sn mineralization in the southwestern South China Block: A case study of the Dulong Sn-dominant polymetallic deposit. Ore Geol. Rev. 93, 268–289.

Zhao, P.L., Xu, C., William-Jones, A.E., Mao, J.W., Yuan, S.D., 2022. The role of phyllosilicate partial melting in segregating tungsten and tin deposits in W-Sn metallogenic provinces. Geology 50, 121–125.

Zhou, X.Y., Yu, J.H., O'Reilly, S.Y., Griffin, W.L., Sun, T., Wang, X.L., Tran, M., Nguyen, D., 2018. Component variation in the late Neoproterozoic to Cambrian sedimentary rocks of WS China–NE Vietnam, and its tectonic significance. Precambr. Res. 308, 92–110.

Zhu, G.L., Yu, J.H., Zhou, X.Y., Wang, X.L., Wang, Y.D., 2019. The western boundary between the Yangtze and Cathaysia blocks, new constraints from the Pingbian Group sediments, southwest China Block. Precambr. Res. 331, 105350.